Electronic Supplementary Material (ESI) for Lab on a Chip.
This journal is © The Royal Society of Chemistry 2015

Electronic Supplementary Information

Fast and Safe Microwave-assisted Glass Channel-shaped Microstructures Fabrication

A. Zacheo,[a,b]* A. Zizzari,[a,b] E. Perrone,[b] L. Carbone,[b] G. Giancane,[c] L. Valli,[c] R. Rinaldi,[a,b] V. Arima[b]*

[a] Department of Mathematics and Physics "Ennio De Giorgi", Università del Salento, Via Arnesano, 73100 Lecce (Italy)
[b] NNL, Nanoscience Institute–CNR, Via Arnesano 16, 73100 Lecce (Italy)
[c] Dipartimento di Ingegneria dell'Innovazione, Università del Salento, Via Arnesano, 73100 Lecce (Italy)
*E-mail: antonella.zacheo@unisalento.it; valentina.arima@nano.cnr.it

Table of Contents

• **Microwave heating applied to glass microstructure fabrication: a theoretical discussion..** **page 2**
• **Experimental……………………………………………………………………………..** **page 3**
 Materials…………………………………………………………………………… **page 3**
 Preparation of samples for etching studies in HWB and MW……………………… **page 3**
 Characterization of depth, width and roughness of the etched microstructures…... **page 3**
 Preparation of samples to explain the reduced underetching effects…………..... **page 3**
 Ellipsometry and AFM characterization………………………………………… **page 3**
• **MW heating settings for glass-substrates etching** *(Table S1)***…………………..** **page 4**
• **Etching conditions and etching rates for B-270 and BF glasses** *(Table S2)***……………** **page 4**
• **Cross section optical images of B-270 microchannels** *(Figure S1)***……………………..** **page 5**
• **AFM and Ellipsometry studies** *(Table S3 and Figures S2-S6)***………………………… ……** **page 5**
• **WE Kinetic of Borofloat™ (BF) glass substrates ……………………………………** **page 8**
• **Microchannel depths of BF glasses HWB- and MW-assisted** *(Figure S7)***……………..** **page 9**
• **Cross section optical images of BF microchannels** *(Figure S8)***…………………………** **page 9**
• **AFM images of 200 µm deep BF microchannels** *(Figure S9)***……………………………** **page 10**
• **Temperature and Pressure profile during MW irradiation** *(Figure S10)***……..........** **page 10**
• **Optical and SEM characterization of serpentine-shaped device** *(Figure S11)***…………** **page 11**
• **References……………………………………………………………………………** **page 11**

ESI-1

• Microwave heating applied to glass microstructure fabrication: a theoretical discussion

When electric fields of electromagnetic waves interact with a dielectric medium, three main effects may be promoted *i.e.* electronic, dipolar and conductive polarization mechanisms. The first mechanism is based on the shift of the negative electron cloud around the positive nucleus in a direction opposite to the field. However, in the MW frequency regime, such mechanism is not as significant as dipolar polarization and conduction mechanisms. Such last two electric-field-promoted responses dominate at MW frequencies. Generally, dipolar polarization occurs due to the rotation of permanently polarized dipoles characteristic of dipolar molecules or parts of them. When an electromagnetic wave propagates in free space, the oscillating electric field operates a torque force on a molecular dipole constantly turning it towards electric field direction. Therefore, at those frequencies, dipoles are in a constant state of mechanical oscillation developing heat because of frictional forces. Such effect of energy dissipation (dielectric losses occurring in dielectric materials) results frequency-dependent and specifically increases as the frequency is raised. The ability of a material to convert electromagnetic energy into heat energy at a given frequency and temperature is estimated quantifying the loss factor: $\tan\delta=\varepsilon_r''/\varepsilon_r'$. δ is the sample dissipation factor, ε_r'' the dielectric loss (imaginary term of the relative permittivity), whereas ε_r' represents the dielectric constant (real term of the relative permittivity) which is indicative of a molecule polarizability. ε_r'' and ε_r' are usually frequency- and temperature-dependent. Ionic conduction represents the second decisive mechanism, caused by the alternate motions of free charges (ions) very similar to conduction in electrolytic solutions. Under the electric field influence, ions move through the solution and the increased number of collisions contribute to generate heat. In water, the low degree of viscosity (1.002 mPa·s at 20°C), further contributes to high ionic mobilities and conductivities.[1-7] Hence, as the dielectric heating is not limited by the thermal conductivity of the reaction vessel, only its content will be selectively heated by a localized superheating of any MW-active substance. An improved homogeneity of the heat distribution will thus result. Then, being the etchant solution formed by highly polar molecules like water and acids, the MW heating approach is adaptable to the glass WE process.

In the present work, semispherical glass channels are developed by the fabrication process described in Arima et al.[8] We investigate and propose the utilization of MW as alternative heating methodology to deliver thermal energy to etchants-containing aqueous solutions during the glass substrate WE process. In order to discriminate MW-mediated side-effects and possibly outline differences in the reaction paths, MW-assisted and conventional HWB-based WE procedures are reciprocally compared. The kinetic of the liquid phase etching process towards two distinct classes of solid substrates either made of B-270 or BF glass and aimed at fabrication of microchannels was investigated. A direct comparison between HWB-based and MW-assisted etching procedure at different temperatures and reaction times has been accomplished. WE experimental conditions as the mask thickness/composition and the etchant formula earlier optimized to produce hundreds of micrometer-deep channels with a nanometer-range roughness [9] were adopted.

Materials with low values of loss tangent ($\tan\delta < 0.1$) can be considered essentially transparent to microwaves (*at that frequency*) and will not undergo significant heating. Water, which at characteristic 2.45GHz frequency and room temperature displays a $\tan\delta = 0.123$ [10] at 50GHz of working frequency becomes an extraordinarily high MW-absorbing solvent ($\tan\delta \approx 1.6$), [4, 11, 12] which in airtight reactors can be almost instantly superheated above its atmospheric-pressure boiling point. Upon increasing the temperature, the water loss tangent subsequently decreases to a value as large as 0.4 (at 100°C and 50GHz), which makes water to behave as medium MW-absorbing solvent at high temperatures.[12] Therefore, at working frequencies of 50GHz, water operates as favorable MW-absorbing environment, extremely reactive at the very first instants of MW delivery as the temperature is still low and then, steadily and proportionally sustaining the dielectric heating up to high reaction temperatures. In a similar manner, selective heating of the other individual molecular components dispersed in solution, as non-dissociated molecules of HF or HF_2^-, will contribute to the sample heat. Viceversa, based on the reported data of loss-tangent at 2.45GHz ($\approx 10^{-4}$), the glass substrates can intuitively be assumed as thoroughly MW-transparent.[10]

Electrolytic conductivity associated to mobilities of free inorganic ions will further contribute to *conduction losses* of the water-based environment. Joule heating, due to MW-promoted translation of positive and negative charged ions, is supposed to be enhanced at high working frequencies.[4, 13] This is additionally encouraged by the abatement of the solvent viscosity at high temperature that, whether from one side contributes to reduce the molecular friction, from the other side allows the ionic species to move with as few hindrances.[10]

• Experimental

Materials

Commercially available B-270 and Borofloat^{TM} (BF) glasses, cut in 2.5cm x 2.5cm x 1.1mm (width x depth x height) slides and covered with 450 nm-thick Chromium (Cr) layer (Telic, USA), were used as solid substrates. Acetone, isopropanol, hydrochloric acid (HCl), ammonium fluoride (NH_4F), and hydrofluoric acid (HF) were purchased from Sigma–Aldrich (Taufkirchen, Germany). The resist AZ9260 and the AZ400k developer were purchased from MicroChemicals (Ulm, Germany). The etchant solution was purchased from Poletto Aldo s.r.l. (Noventa di Piave, Venice, Italy).

Preparation of samples for etching studies in HWB and MW

All samples were cleaned with acetone and isopropanol. Then, the resist was deposited and softly baked to remove the solvent. A serpentine pattern (Fig. S11a) with microchannels of 300 µm nominal width, W_M,[8] was transferred from a photo-mask (J.D. Photo-tools Ltd.,Oldham, Lancashire, UK) to the photoresist layer by exposing samples to UV light. Immediately after exposure, development was done in diluted AZ400k at room temperature and rinsing with pure water subsequently. The underlying Cr film was removed using the etchant solution. A one hour long hard-baking process was then performed to harden the photoresist against attacks of etchants.
Exposed glasses were then etched with a BOE solution consisting of NH_4F dissolved in pure water to obtain a 1,38 M solution and then added to HF (48%) and HCl (38%) to obtain HF:NH_4F: HCl 1:41: 1 ratio. The HF final concentration was 4.7%. Afterwards, the glass substrates were wet-etched in the BOE solution either using a HWB or a MW reactor system, the latter operating at a frequency of 50 GHz (Anton Paar Multiwave 3000, Labservice Analytica s.r.l., Italy). According to HWB-based approach, a teflon-made tray containing a freshly-prepared BOE solution is immersed into a temperature-controlled water bath. Afterwards, the sample is dipped into the BOE solution at the set temperature value (etching-time-zero). On the contrary, in the case of MW-based experiments, four closed vessels (one used as reference and three with the samples) were used in the MW rotor with an optimal working volume of 30 mL for each vessel. A pressure/temperature (PT) sensor is inside a reference vessel (only the BOE solution containing), whereas the temperature inside each sample-containing rotating vessel is monitored by an infrared ray temperature sensor. The temperatures herein reported are referred to the PT sensor (Fig. S10).
After the WE process, the UV unexposed layer of photoresist and its underlying Cr film were definitely removed with acetone and Cr etchant solution respectively.

Characterization of depth, width and roughness of the etched microstructures

After WE treatments, the resulting channel depths and widths were verified by using a profilometer (Dektak 6M Stylus Profiler Digital Instrument-VEECO) and an inverted optical microscope system (NIKON Eclipse Ti, mod. DS-5MC camera, ND2 software system). The depth values reported in the graphs (Fig. 1 in the main paper) are an average over 10 microchannels for each etched sample (n=3 samples, about 30 measurements, for each time point) and the error calculated as standard deviation. Moreover the surface roughness of 200 µm deep channels etched at 70°C in HWB for 35 min, and at 70°C for 45 min, 100°C for 20 min and 150°C for 5 min in MW was evaluated by Atomic Force Microscope, AFM (Nanoscope IIIa, Veeco, USA) and the values reported are an average over 10 measurements acquired on 3 µm x 3 µm areas.

Preparation of samples to explain the reduced underetching effects

Possible effects of the BOE solution and of the MW on the Cr layer properties have been investigated by immersion of four B-270 glass substrates, covered by a 450 nm-thick Cr layer, in the BOE solution respectively at room temperature and at 50°C, 100°C and 150°C under MW radiation. After 5 min of reaction, the samples were washed with pure water, dried with N_2 and characterized by Ellipsometry to determine the Cr thickness (see Fig. S3-S6).
After analysis, the four samples, along with an original non-etched Cr-coated substrate, were immersed in a Cr etchant solution for some minutes, until the Cr was completely removed from the untreated sample. After the reaction, all the samples were washed with pure water, dried with N_2 and further characterized by Ellipsometry and AFM (see Fig. S2).

Ellipsometry and AFM characterization

A Nanofilm EP4 Ellipsometer was used to measure the Cr layer thickness and evaluate the possible diffusion of Cr atoms in the glass substrate. All measurements were carried out varying the angle of incidence from 45° to 60° with a step size of two degrees and changing the wavelength from 380 nm to 900 nm.
The Cr mask interactions with the glass substrate after 5 min at 50°, 100° and 150°C in MW, were investigated by AFM analysis (Nanoscope IIIa, Veeco, USA). Topographic images were acquired in tapping mode using silicon cantilevers (model RFESPA) with a tip radius of 8 nm and a resonance frequency of 70–85 kHz.

• MW heating settings for glass-substrates etching

Heating Temperature (°C)	Heating Ramp (s)	Heating Power (W)	Cooling Time (min)	Pressure (bar)
50	90	600	0	0.80
70	120	600	2	0.80
100	120	600	8	0.85
150	180	800	12	4.50

Table S1. MW heating settings for glass-substrates etching. The reported pressure is the value reached during the etching reaction time (see Fig. S10)

• Etching conditions and etching rates for B-270 and BF glasses

Etching conditions		Etching rate (μm/min)	
Etching Temperature (°C)	**Heating method**	**B-270**	**BF**
50	HWB	4.0 ± 0.1	0.20 ± 0.01
50	MW	6.7 ± 0.1	0.30 ± 0.01
70	HWB	7.4 ± 0.1	0.50 ± 0.01
70	MW	12.0 ± 0.2	0.70 ± 0.01
100	MW	22.5 ± 0.3	2.50 ± 0.01
150	MW	40.5 ± 0.3	16.7 ± 0.3

Table S2. Summary of the etching conditions used for B-270 and BF glasses and calculation of etching rates within the first 5 min of treatment.

• Cross section optical images of B-270 microchannels

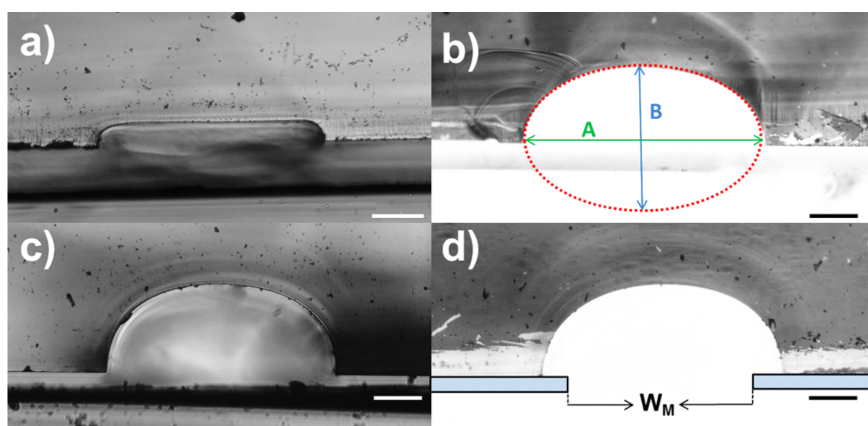

Figure S1. Optical images report the cross sections of B-270 microchannels of similar wet-etched width (W_E) in MW at **a)** 50°C -25 min, **b)** 70°C-25 min, **c)** 100°C-10 min and **d)** 150°C-5 min. At 50°C, the vertical etching rate is yet too low to display effects of underetching. Whereas, at 70°C or higher temperatures, an ellipsoid-fitting can be performed (**b**) in order to show the channel etching development, with the estimated A/B ratio (that is $W_E/2D_E$) designating the ratio of the major axis (A= W_E) to the minor one (B= $2D_E$). Comparing the A/B ratios of microchannels of similar W_E at 70°C (A/B=1.5, **b**), 100°C (A/B=1.3, **c**) and 150°C (A/B=1.3, **d**), it is confirmed that the aspect ratio decreases at higher etching temperatures and stabilizes around 100°C due to minimization of underetching effects as well as enlargement of the channel height. In picture **d)** W_M refers to photo-mask channel width.

• AFM and Ellipsometry studies

Heating Temperature (°C)	Thickness (nm)	Error (nm)	RMSE
r.t.	455	8	1.3
50	432	10	0.9
100	421	12	1.6
150	419	12	1.1

Table S3. Samples thickness calculated by means of ellipsometric data. Under such MW heating conditions in BOE solution, the temperature effect induces a decrease of the Cr layer thickness and a modest thinning of the Cr mask takes place. The measurements evidence that the MW treatment reduces the Cr layer thickness and, specifically, such reduction of the metallic film is relevant already at a heating temperature of 50°C, *i.e.* 23 nm thinner than original value. Then, the metallic thickness does not substantially change for higher heating temperatures as 100°C or 150°C.

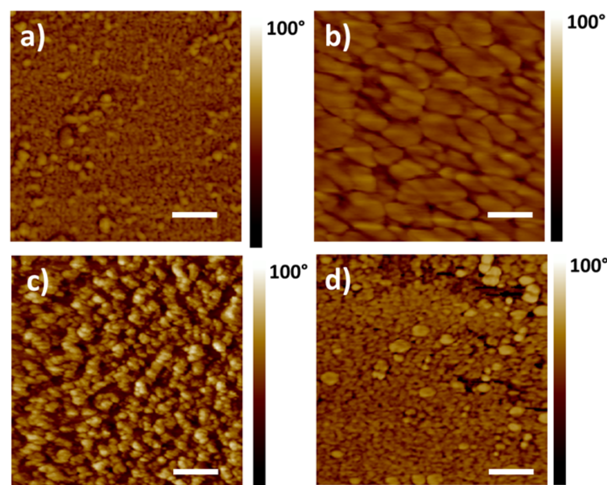

Figure S2. Phase images of B-270 samples treated with Cr etchant for 5 min, **a)** without any previous MW heating, and after 5 min MW heating respectively at **b)** 50°C, **c)** 100°C, and **d)** 150°C. Scale bar is 2 µm. The morphologies of samples treated in MW and then with Cr etchant were compared with those of samples in which only Cr removal without any MW heating was performed. As shown in these phase contrast AFM images, small and low density round shape clusters are observed on the top of non-heated samples (**a**), which probably represent residues of Cr on the glass substrate. The removal of Cr in samples treated at 50°C in MW shows micrometer-sized flat agglomerates covering the substrate surface (**b**); no glass-related features are recognizable on the substrate. At 100°C (**c**), smaller clusters are visible, with a higher density coverage. The flat cluster become even smaller and the substrate coverage larger at 150°C of heating treatment. The presence of these clusters, reasonably attributable to Cr residues, is denser for samples treated in MW than in non-heated ones. This means that, the Cr etchant treatment is more effective for non-heated samples as the Cr attachment to the substrate becomes stronger after the MW treatment even if a thinning of the Cr film is observed. To confirm that the clusters visible in **b-d** are due to Cr residues well attached to the glass substrate, some studies of the dielectric properties of these samples were performed by Ellipsometry. A Maxwell-Garnett effective medium approximation [14, 15] was used to estimate the anisotropy inclusions of Cr atoms into the glass substrate. In the sample treated at 150°C (whose morphology is shown **d**) a percent of 2.1 ± 0.8 of Cr in the first 60 nm was measured, confirming the previously proposed rationale; on the contrary, no Cr was found on samples treated with Cr etchant at room temperature (sample shown **a**).

In order to evaluate the thickness of the Cr layers, a Drude model has been used to fit the ellipsometric data. The measurements have been carried out varying the incident angle from 48 to 72 degrees. The incident beam wavelength has been set at 512 nm. In figures S3-S6 the experimental data and the simulated curves are reported for Δ and Ψ for the samples treated at RT, 50 °C, 100 °C and 150 °C, respectively.

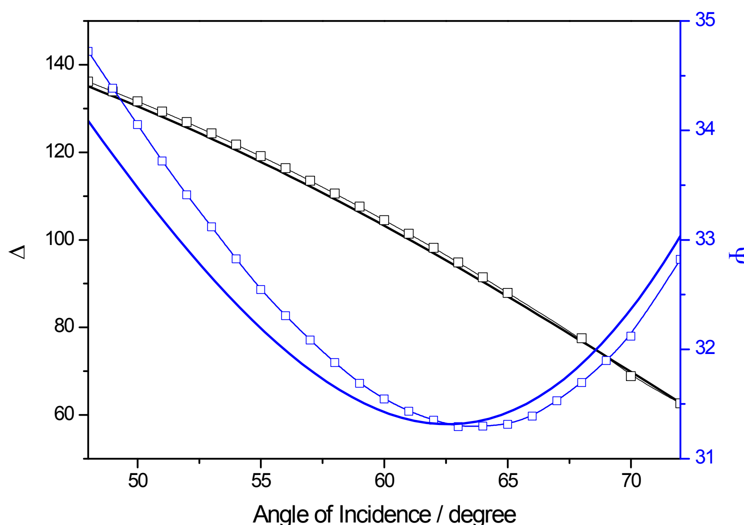

Figure S3. Experimental (symbols) and simulation curve (continuous line) of Δ and Ψ for the Cr layer of a sample treated at r.t. in BOE solution. Calculated thickness is (455±8) nm with a RMSE of 1.3.

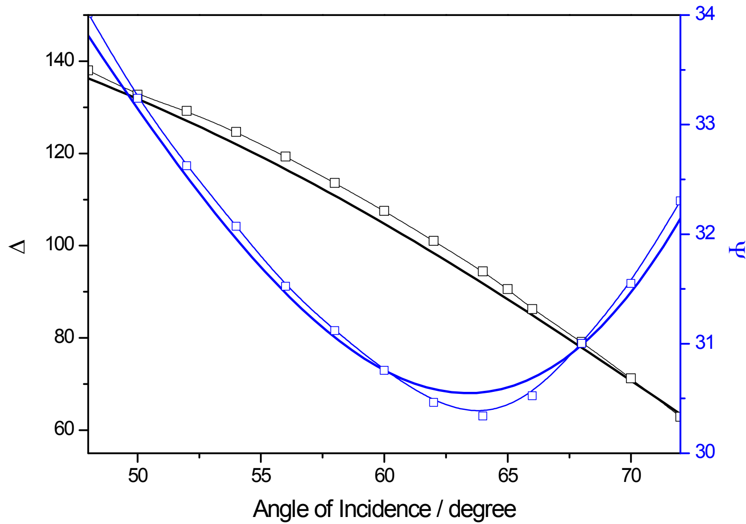

Figure S4. Experimental (symbols) and simulation curve (continuous line) of Δ and Ψ for the Cr layer of a sample heated at 50°C in MW in BOE solution. Calculated thickness is (432±10) nm with a RMSE of 0.9.

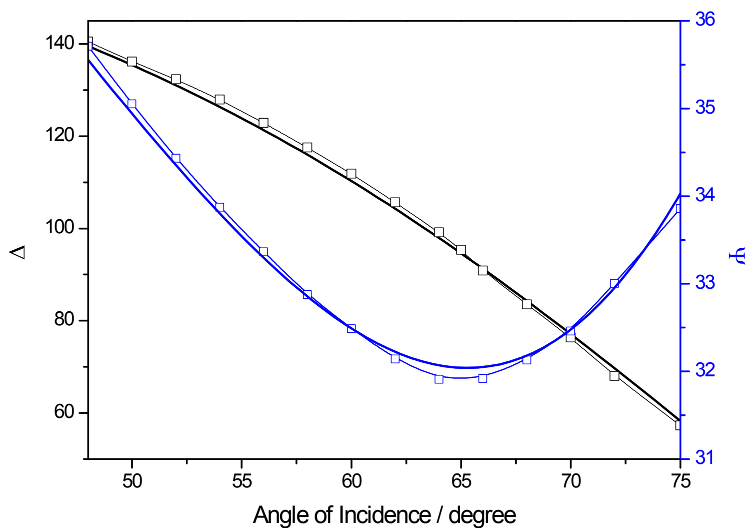

Figure S5. Experimental (symbols) and simulation curve (continuous line) of Δ and Ψ for the Cr layer of a sample heated at 50°C in MW in BOE solution. Calculated thickness is (421±12) nm with a RMSE of 1.6.

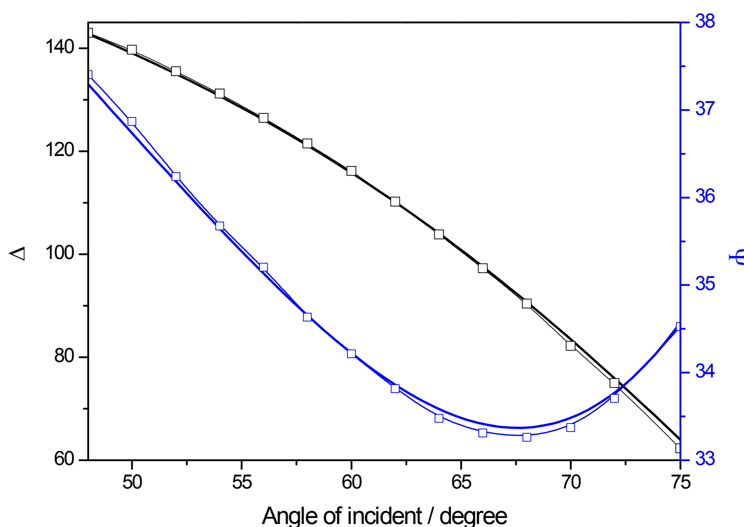

Figure S6. Experimental (symbols) and simulation curve (continuous line) of Δ and Ψ for the Cr layer of a sample heated at 50°C in MW in BOE solution. Calculated thickness is (419±12) nm with a RMSE of 1.1.

• WE Kinetic of Borofloat ™ (BF) glass substrates

To demonstrate the wide applicability of this technique, the WE method, under MW employment, was applied to another kind of glass, widely used in microfabrication, namely the Borofloat (BF). The same experimental trends were observed in kinetic studies at 50° and 70°C in HWB and at 50°, 70° and 100°C in MW (see Fig. S7a). MW-induced chemical etching was performed at 50°C, 70°C, 100°C and 150°C for 5 min (Fig. S7b, red line). A comparison between Fig. 1(a-b) in the main paper and Fig. S7(a-b) and data reported in Table S2 demonstrate that the WE rates for BF glasses were lower than for B-270 glasses because of the stabilizing properties of the B_2O_3 in BF glass. [16] Additionally, a higher reproducibility of the BF etching was observed as, calculated errors are in the range of tens of nanometers. Compared with the curves of Fig. 1a in the main paper, those observed in Fig. S7a exhibit a more linear behavior as the amount of etching products is limited. Results reported in Fig. S7b, plot on the left side, black line, show that deeper channels can be produced also for BF at higher temperatures with reduced underetching effects. As expected, faster etching rates at higher temperatures produce lower values of R, with a rounded channel profile (see Fig. S8).
The effect on the roughness and on the morphology was also evaluated by comparing samples of similar depth produced at 70°C in HWB and 150°C in MW (see AFM images of Fig. S9). The values were 0.79 ± 0.07 nm in MW and 0.74 ± 0.10 nm in HWB and, unlike B270 glasses, show for BF the independence of the roughness from the etching temperature and the heating modality. This can be due to chemical composition of BF and the significantly reduced etching rate.
Indeed, by increasing the reaction temperature up to 150°C, it's possible to speed up the etching rate fiftyfold respect to 50°C treatment (16.7 μm/min vs 0.3μm/min, respectively; see Table S2), and, at the same time, to decrease *R* without meaningful influence on the roughness of the microchannels.

• Microchannel depths of BF glasses HWB- and MW-assisted

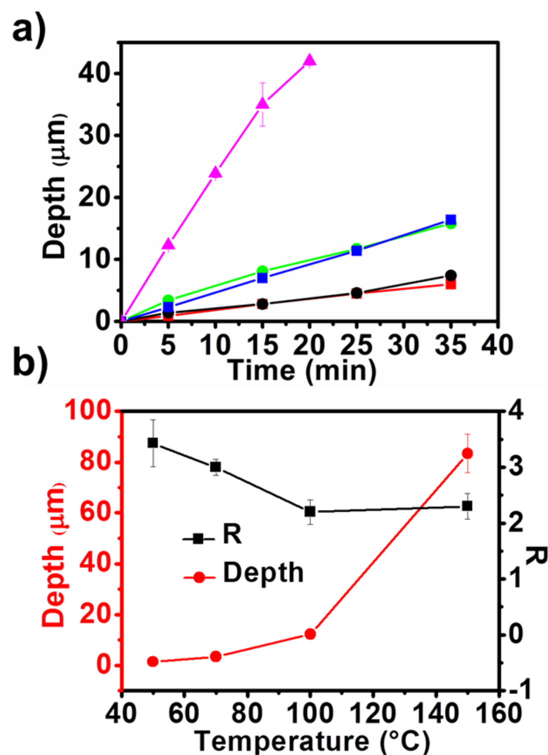

Figure S7. a) Channel depth of BF glasses etched in BOE solution as function of the etching time and temperature in HWB (50°C red line and 70°C blue line) and MW (50°C black line, 70°C green line, and 100°C magenta line. **b)** Left side: the red curve shows the depth of B-270 microchannels etched for 5 min at different temperatures. Right side: the black curve displays the ratio *R* of samples etched for 5 min at different temperatures.

• Cross section optical images of BF microchannels

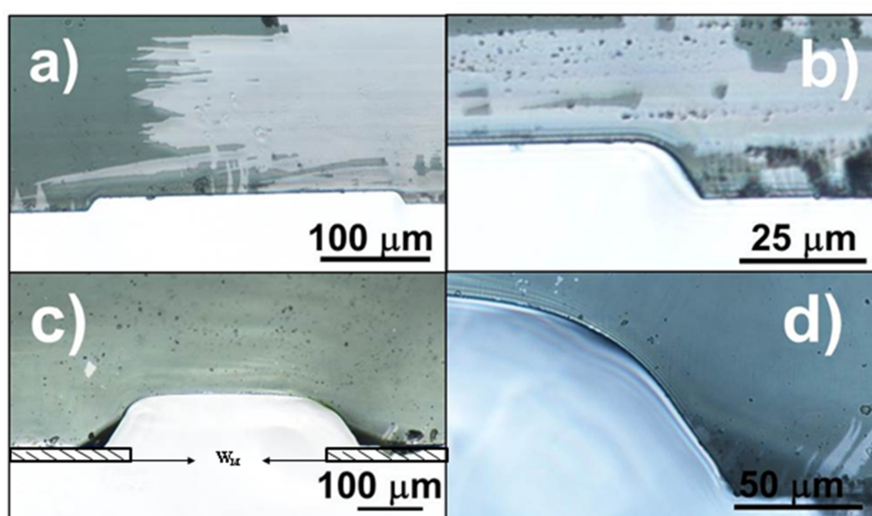

Figure S8. Optical images of the cross section of BF microchannels of similar width produced in MW at a) 50°C, b) 70°C, c) 100°C and d) 150°C. In picture c) W_M refers to photo-mask channel width.

• AFM images of 200 µm deep BF microchannels

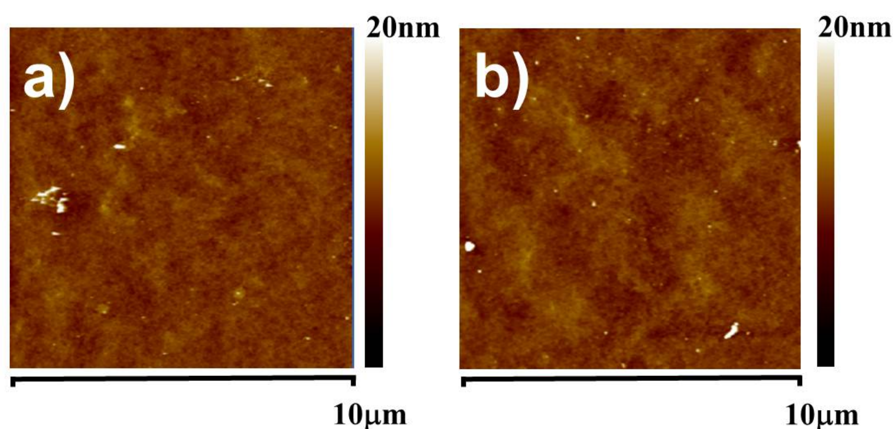

Figure S9. AFM images of 200 µm deep BF micro-channels respectively treated at a) 70°C in HWB and b) 150°C in MW.

• Temperature and Pressure profile during MW irradiation

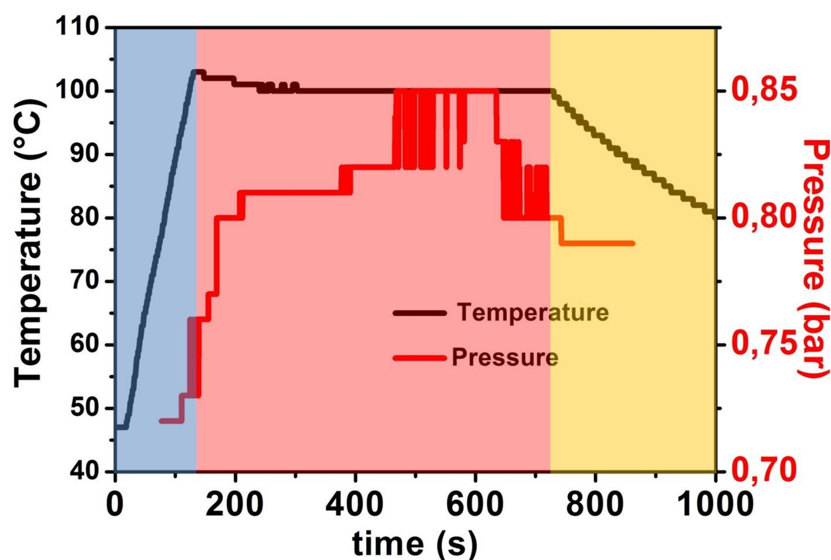

Figure S10. Example of temperature (left side, black curve) and pressure (right side, red curve) profiles for MW heating at 100°C. For the sake of clarity, the depths of etching emerging from MW experiments, develop from sample reactivity occurring during three consecutive reaction steps: 1) the **heating ramp** (blue area) which is the time period to reach the set temperature, 2) the **reaction time** (red area) at the fixed temperature (100°C in this example) and finally 3) the **cooling time** (yellow area) during which the system undergoes a gas-jet-promoted cooling.

• Optical and SEM characterization of serpentine-shaped device

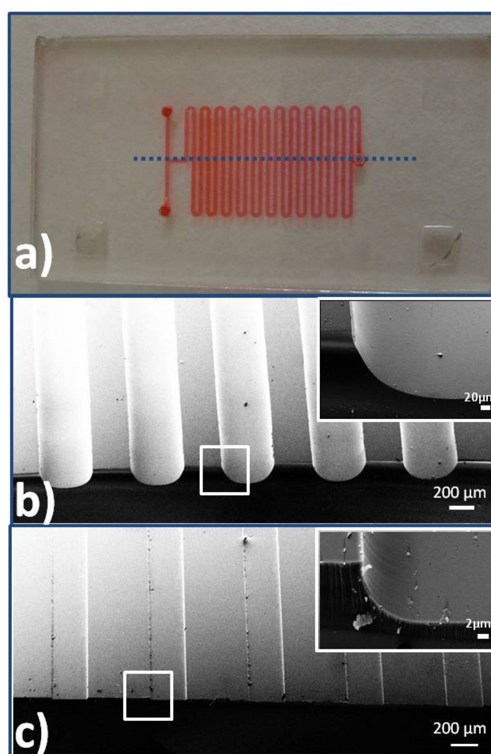

Figure S11. a) Optical image of the entire serpentine device filled with a red solution to better display the geometry of the chip (blue dashed line show the level where the device was cut for channel profile characterization. Example of SEM pictures showing the cross section of 175 µm deep channels for B270 (**b**) and 12 µm deep channels for BF (**c**), produced in MW at 100° for 10 min and at 70°C for 25 min respectively. The insets show higher-magnification SEM images of the channel sections highlighted by the square.

• References

1. P. Lidstrom, J. Tierney, B. Wathey and J. Westman, *Tetrahedron*, 2001, **57**, 9225.
2. S. P. Tripathy, R. V. Kolekar, C. Sunil, P. K. Sarkar, K. K. Dwivedi and D. N. Sharma, *Nucl Instrum Meth A*, 2010, **612**, 421-426.
3. M. Ahmad and G. W. Grime, *Microscopy and Microanalysis*, 2013, **19**, 261-267.
4. C. Gabriel, S. Gabriel, E. H. Grant, B. S. J. Halstead and D. M. P. Mingos, *Chem Soc Rev*, 1998, **27**, 213-223.
5. V. Ragaini, C. Pirola, S. Borrelli, C. Ferrari and I. Longo, *Ultrason Sonochem*, 2012, **19**, 872-876.
6. M. Baghbanzadeh, L. Carbone, P. D. Cozzoli and C. O. Kappe, *Angew Chem Int Edit*, 2011, **50**, 11312-11359.
7. E. T. Thostenson and T. W. Chou, *Compos Part a-Appl S*, 1999, **30**, 1055-1071.
8. V. Arima, G. Pascali, O. Lade, H. R. Kretschmer, I. Bernsdorf, V. Hammond, P. Watts, F. De Leonardis, M. D. Tarn, N. Pamme, B. Z. Cvetkovic, P. S. Dittrich, N. Vasovic, R. Duane, A. Jaksic, A. Zacheo, A. Zizzari, L. Marra, E. Perrone, P. A. Salvadori and R. Rinaldi, *Lab on a Chip*, 2013, **13**, 2328-2336.
9. N. Pekas, Q. Zhang, M. Nannini and D. Juncker, *Lab on a Chip*, 2010, **10**, 494-498.
10. C. O. Kappe, *Chem Soc Rev*, 2013, **42**, 4977-4990.
11. R. Buchner, J. Barthel and J. Stauber, *Chem Phys Lett*, 1999, **306**, 57-63.
12. J. B. Hasted, *Ed. F. Franks (Plenum Press, New York*, 1972, **1**, 255-309.
13. T. W. Dakin, *IEEE Electrical Insulation Magazine*, 2006, **22**, 11-28.
14. G. Maxwell and J. C., *Philos. Trans. R. Soc. London*, 1904, **3**, 385-420.
15. M. Y. Koledintseva, R. E. Dubroff and R. W. Schwartz, *Prog Electromagn Res*, 2006, **63**, 223-242.
16. G. A. C. M. Spierings, *J Mater Sci*, 1993, **28**, 6261-6273.